Applied Physics Letters

Highly sensitive hydrogen detection using curvature change of wireless-electrodeless quartz resonators

Cite as: Appl. Phys. Lett. **115**, 171901 (2019); https://doi.org/10.1063/1.5126135
Submitted: 29 August 2019 . Accepted: 05 October 2019 . Published Online: 21 October 2019

L. Zhou, N. Nakamura, A. Nagakubo, H. Ogi, et al.

Applied Physics Letters ARTICLE scitation.org/journal/apl

Highly sensitive hydrogen detection using curvature change of wireless-electrodeless quartz resonators

Cite as: Appl. Phys. Lett. **115**, 171901 (2019); doi: 10.1063/1.5126135
Submitted: 29 August 2019 · Accepted: 5 October 2019 ·
Published Online: 21 October 2019

L. Zhou,[1] N. Nakamura,[2] A. Nagakubo,[1] and H. Ogi[1,a)]

AFFILIATIONS

[1]Graduate School of Engineering, Osaka University, 2-1 Yamadaoka, Suita, Osaka 565-0871, Japan
[2]Graduate School of Engineering Science, Osaka University, Toyonaka, Osaka 560-8531, Japan

[a)]ogi@prec.eng.osaka-u.ac.jp

ABSTRACT

We propose a hydrogen detection method using a thin quartz resonator with a palladium thin film on its single side, which absorbs hydrogen, resulting in the film expansion and geometry change of the resonator, shifting the resonant frequency. Because the resonator is driven in a wireless manner, the other resonator side can remain electrodeless, enhancing the geometry change and then the detection sensitivity. The detection limit is 1 ppm or less. We also investigate the reaction kinetics between palladium and hydrogen through the temperature dependence of the reaction velocity constant, yielding the activation energy of 0.372 ± 0.003 eV. This is close to the activation energy for the hydrogen-atom transition from the surface to subsurface states, indicating that the adsorption reaction is dominated by the transition rather than the bulk diffusion in palladium.

Hydrogen has been considered as an ideal energy carrier because of its high energy density and zero-emission property, and its concentration monitoring is important to control the reactions. Reliable and fast detection of hydrogen leakage remains a critical issue for safety in advancing energy application of hydrogen.[1] Therefore, many types of hydrogen sensors have been developed.[2–7] A majority of existing hydrogen sensors utilize palladium as the sensing material. Palladium selectively absorbs hydrogen gas[8,9] and causes volume expansion because hydrogen atoms occupy the interstitial sites. This mechanism has been used for hydrogen detection through measuring the change in resistance of semicontinuous palladium films[10,11] and palladium mesoscopic wire arrays,[12] surface stress,[13] and bending deformation[14] of cantilever, resonant frequency of a beam resonator,[15] and wavelength of fiber Bragg gratings.[16,17] The limit of detectable hydrogen concentration, however, ranges from several hundred parts per million to a few percent in most previous studies. Although lower detection limits of 25 ppm (Ref. 18) and 27 ppm (Ref. 19) have been achieved, further sensitivity improvement is needed.

In this Letter, we propose an advanced hydrogen detection method using wireless-electrodeless AT-cut quartz resonators.[20,21] We deposit a palladium thin film on one surface side of the quartz plate, leaving the other surface uncoated. When the resonator is exposed to hydrogen gas, bending of the resonator occurs because of the palladium-film expansion, resulting in the change in its resonant frequency. (The effect of the geometry change on resonant frequencies of beam resonators has been reported.[22,23]) Because the expansion of the palladium film highly depends on the hydrogen-gas concentration, monitoring the frequency response can provide us with the concentration and also the kinetics of the binding reaction between palladium and hydrogen. Acoustic methods were also previously proposed using palladium and its alloy thin films attached on the propagation paths.[24–27] Yamanaka *et al.*,[25,26] for example, developed the ball surface-acoustic-wave sensor, achieving fast response time. However, the existing acoustic methods detect the gas absorption through a change in properties (mass density, elasticity, and anelasticity) of the propagation medium, which slightly affects the macroscopic acoustic response. Therefore, ultrasensitive detection of hydrogen remains difficult. (The detectable hydrogen concentration in acoustic methods was ~10 ppm or higher.)

It is worth pointing out that our sensing mechanism is difficult to be performed using conventional quartz-crystal-microbalance (QCM) sensors, where palladium electrodes are required on both surfaces, restricting the bending deformation of the quartz resonator. Combined with the wireless-electrodeless QCM technology, highly

sensitive detection of hydrogen with the concentration as low as 1 ppm is achieved. Moreover, interaction between hydrogen gas and palladium is of fundamental importance for both industrial applications and basic research.[28,29] We investigate the kinetics of hydrogen attachment on the palladium surface and its diffusion into the palladium lattice through the subsurface region. We determined the activation energy of the adsorption reaction, which shows good agreement with that of the surface-to-subsurface transition of the hydrogen atom.

Figure 1(a) shows the wireless-electrodeless quartz-resonator sensor cell,[20,30] in which an AT-cut quartz resonator is lightly sandwiched by two silicon-rubber gaskets. Its shear vibration is driven by the line antenna for excitation, and the resonator oscillation is detected by the other antenna. The resonant frequency is monitored by the transmission coefficient (S12 parameter) using a vector network analyzer with a power consumption of 10 dBm. The through-thickness shear-mode fundamental resonant frequency is 64.5 MHz (26 μm thick). The in-plane dimensions are 2.5 mm × 1.7 mm. The thin films were deposited using the radio frequency (RF) magnetron-sputtering method. We deposited a 5-nm chromium thin film and then a 200-nm palladium thin film on the resonator surface at 400 °C. The base pressure of the chamber was ~1×10^{-6} Pa, and the argon pressure during deposition was 0.8 Pa. We measured the film thickness by the X-ray total reflectivity measurement,[31] which allows determination of the film thickness within 1% error. As shown in Fig. 1(b), we flow high purity (99.9999%) nitrogen gas to the sensor cell as the carrier gas at a flow rate of 100 ml/min. Then, a hydrogen gas sample diluted by the high-purity nitrogen gas is injected, which is mixed with the carrier nitrogen gas, entering the sensor cell at the intended concentration. In all experiments, the exposure time to hydrogen gas is 140 s. The sensor cell is placed on a heater to perform the measurements between 40 and 55 °C. Because the measurement at 55 °C showed the maximum frequency response as will be shown, we principally performed the hydrogen-gas-detection experiments at 55 °C. (Because higher temperature caused damage in our sensor cell, we performed measurements below 55 °C.)

Figure 2(a) shows the frequency changes observed for injections of hydrogen gas with the concentration ranging from 1 to 250 ppm. When the hydrogen gas arrives at the resonator surface, the resonance frequency significantly decreases, and it recovers to the baseline by replacing with the carrier nitrogen gas, releasing hydrogen atoms from palladium. We repeated the experiment three times independently.

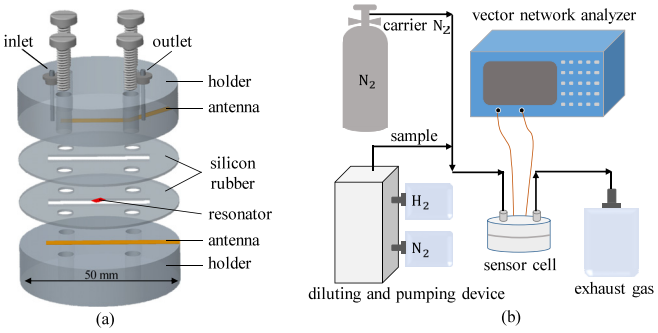

FIG. 1. (a) Illustration of the sensor cell. The AT-cut quartz resonator (red) is lightly sandwiched by the silicon-rubber gaskets. (b) Appearance of the flow-injection system for the hydrogen-gas sensing.

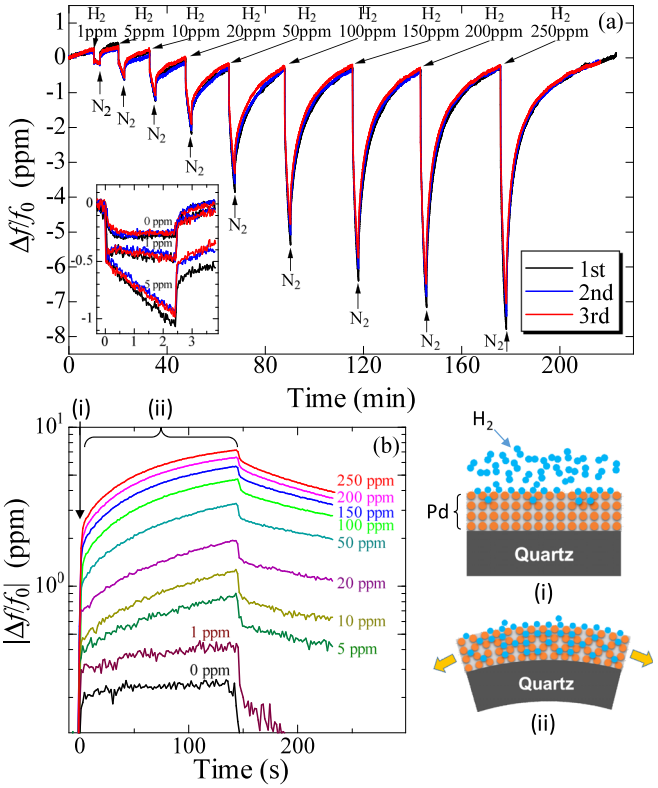

FIG. 2. (a) Frequency response of the 64.5 MHz quartz resonator upon exposure to hydrogen gas with various concentrations. Three repeated experimental results are shown in different colors. The inset shows the enlarged frequency responses to hydrogen gas with concentrations of 0, 1, and 5 ppm. (b) Frequency response curves in the second experiment in (a). Illustrations near the surface for (i) before injection and (ii) during the frequency change are shown.

The frequency shifts are reversible and highly reproducible. For a clearer comparison, we plot the binding and dissociating curves of the second experiment in Fig. 2(b), showing that the amount of the frequency change increases as the hydrogen-gas concentration increases and its limit of detection is 1 ppm or less.

One may attribute the frequency decrease in Fig. 2 to the mass loading effect, which has been recognized as the principal mechanism in QCM sensors.[32] However, we find that the crystal curvature should be the essential mechanism for the frequency decrease. In order to confirm this, we fabricated another resonator where the palladium films were deposited on both sides. (We needed to reduce the palladium area on one side to maintain the electric disconnection between the two sides.) In this case, the volume expansion of palladium on both sides restricts the bending deformation of the resonator (although bending deformation occurs because of the different palladium areas on the two sides), whereas the mass loading effect could be enhanced. Figure S1 compares the frequency changes observed with the two resonators having the palladium film only on a single side and on both sides. The frequency changes of the resonator with the palladium films on both sides are nearly half those of the one-side resonator, which cannot be explained by the mass loading effect because it should have caused a larger frequency change.

We then calculated the resonance frequency change caused by the resonator curvature using the finite-element-method (FEM) calculation. (The calculation details are given in the supplementary material.) Figure 3 shows the relationship between the curvature and the fundamental through-thickness shear resonant frequency. For isotropic materials (aluminum and isotropic quartz), the resonance frequency is almost independent of the curvature. However, in the AT-cut resonator, it significantly decreases with the increase in the curvature because of crystal's anisotropy. Also, an important finding is that they show an approximately linear relationship as shown in the inset in Fig. 3. The frequency change due to the geometry change can be enhanced in the anisotropic material such as quartz crystals (Fig. 3), and this effect is more significant than the stress effect.[15]

The hydrogen absorption reaction involves three steps.[33,34] (i) When the palladium-coated quartz resonator is exposed to hydrogen gas, hydrogen molecules are attached and dissociated on the palladium surface. The first reaction for attachment and dissociation is expected to proceed in a short time because the binding state of the hydrogen atom on palladium is sufficiently stable.[35,36] (ii) The hydrogen atoms then penetrate from the surface to the subsurface region.[36,37] (iii) They migrate inside the palladium lattice to cause the bulk diffusion. When the hydrogen content, n, is small ($\lesssim$0.025 at 55 °C), α palladium hydride (PdH_n) is stably formed, resulting in the volume expansion,[8,38] causing the curvature of the resonator, and then decreasing the resonant frequency. The hydrogen content at the saturation state in palladium follows Sievert's law,[39] $n_{sat} = \sqrt{P_{H_2}}/K_s$, where P_{H_2} is the hydrogen-gas partial pressure in Torr and K_s is Sievert's constant (360 $Torr^{1/2}$ at 323 K).[40,41] This equation estimates the maximum possible hydrogen content of 0.001 at a hydrogen-gas concentration of 250 ppm, and this is much smaller than the critical content (0.025) for stable α palladium hydride, beyond which the β palladium hydride would appear. Therefore, we consider that our experiments have been performed under the α palladium hydride state. Along with the hydrogen absorption reaction, the hydrogen discharge reaction proceeds as follows: hydrogen atoms captured inside palladium immigrate to the surface through the subsurface, they recombine into molecules, and they are released from the palladium film. The hydrogen absorption and discharge reactions thus proceed at the same time, and, in the flow-injection system, which keeps the hydrogen-gas concentration constant during the reactions, the reactions will follow the pseudo-first-order reaction with the reaction-velocity constants k_a and k_d for absorption and discharge reactions. In this case, the hydrogen content $n(t)$ in the palladium lattice changes with time t exponentially:[42,43] $n(t) = n_{sat}\{1 - \exp[-(k_a C_{H_2} + k_d)t]\}$, where C_{H_2} denotes the hydrogen-gas concentration. (It should be noted that k_a and k_d indeed involve the multiple reaction mechanisms and they are apparent reaction constants when we simply treat the reactions with single steps.)

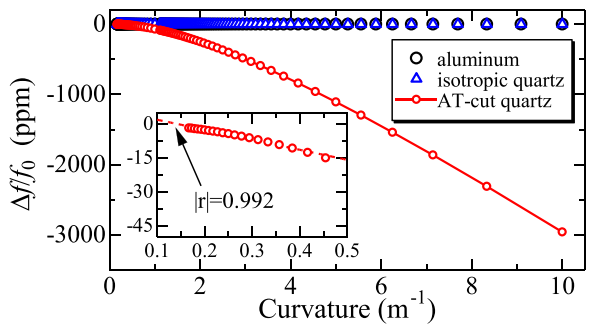

FIG. 3. FEM calculation results of the frequency change for quartz and aluminum resonators as a function of the resonator curvature. The inset shows the enlargement of the frequency change of the AT-cut-quartz resonator at low curvatures.

The palladium-coated quartz resonator undergoes biaxial bending because of hydrogen absorption and expansion of the palladium film. The linear expansion strain ϵ is expressed by the hydrogen atomic content as $\epsilon = 0.026 \cdot n(t)$ for α palladium hydride.[44] The curvature of the resonator under the biaxial strain condition is proportional to the film eigen strain,[45] and we find it is also approximately proportional to the frequency change (Fig. 3). Therefore, the frequency change $\Delta f(t)$ is proportional to the hydrogen content, yielding $(\Delta f(t)/f_0) \propto \{1 - \exp[-(k_a C_{H_2} + k_d)t]\}$, where f_0 denotes the baseline resonance frequency.

Figure 4(a) enlarges the typical frequency response after the arrival of the sample hydrogen gas. We first observe the steep frequency drop and then the nearly linear frequency decrease. The first steep drop will be attributed to the first hydrogen attachment on the palladium surface as discussed above. However, a small frequency drop is always observed even in the 0-ppm hydrogen gas (nitrogen gas) injection as shown in Fig. 4(a), and a part of this drop is caused by the baseline shift because of additional injection pressure. Therefore, we focus on the frequency change after the drop. Because it takes a long time for the frequency change to be saturated during the hydrogen-gas flow, we use the initial frequency response for the analysis by approximating the frequency change with a linear form,

$$\frac{\Delta f(t)}{f_0} = -A(k_a C_{H_2} + k_d) \cdot t, \tag{1}$$

where A is a constant. The sensitivity of our quartz resonator hydrogen sensor is thus defined as the slope of the frequency change after the fast frequency drop [dashed line in Fig. 4(a)] because it is proportional to the hydrogen-gas concentration C_{H_2} [Eq. (1)]. Figure 4(b) shows the relationship between the frequency slope and the hydrogen-gas concentration, showing good correlation. The limit of

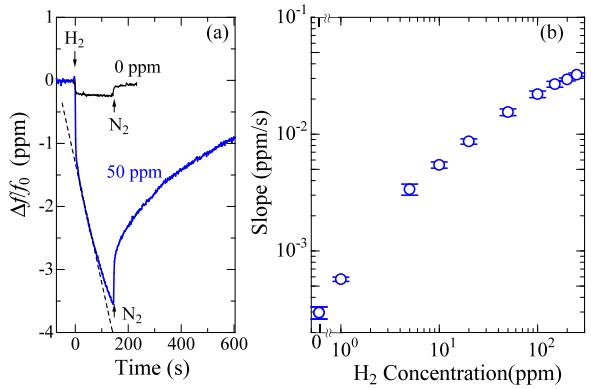

FIG. 4. (a) Frequency responses for injections of 0-ppm and 50-ppm hydrogen gas samples and least-squares-fitted line (dashed line). (b) Relationship between the frequency-change slope and the hydrogen concentration. The error bars indicate the standard deviation of three repeated experiments.

TABLE I. Performance comparison of typical hydrogen detection methods.

Sensing mechanism	Temperature (°C)	Detection limit	Response time	Recovery time
Resistance of the Pd thin film[4]	25–100	600 ppm	200 s (100 °C)	200 s (100 °C)
Frequency of the Pd-coated beam resonator[15]	…	<0.5%	∼1 s	∼90 s
Conductance of Pd nanoclusters[18]	Room temperature	25 ppm	68 ms (2% H_2)	…
Conductance of Pd nanowires[19]	Room temperature	27 ppm	5–30 s	∼20 s
Attention of the surface acoustic wave[46]	Room temperature	10 ppm	20 s	∼10 min
Pd-coated fiber Bragg grating[47]	75	100 ppm	≤ 42 s	166 s
Resistance of the Pd/Ag thin film[48]	80–180	100 ppm	108 s (0.01% H_2)	<120 s
PdNPs/SiO2/Si MOS capacitor[49]	Room temperature	1%	1.2 s	10 s
Pd/SiO2/Si MOS capacitor[50]	Room temperature	1%	1.4 s	14 s
This work	55	≤ 1 ppm	3–100 s	∼20 min

the detectable concentration is 1 ppm or less. As mentioned above, this limit of detection is highly superior to those of existing methods (≳ 20 ppm), involving acoustic methods (≳ 10 ppm).

In our method, the hydrogen-gas concentration is evaluated from the initial slope of the frequency decrease. The response time is defined as the time needed for reliably determining the slope. It is about 100 s for 1 ppm hydrogen gas. For a higher concentration (250 ppm), the response time can be reduced to ∼3 s. The time for recovery is about 20 min when the frequency returns to 90% of the baseline level. Table I compares the specifications for hydrogen-gas detection in this work with those of previously reported methods. Although the recovery time is not competitive, our method still shows superior performance because of its comparable operating temperature and response time and much lower detection limit.

Another important subject is the evaluation of the effective activation energy of the hydrogen absorption reaction with palladium. Owing to the linear relationship between the frequency change and the reaction velocity constant k_a, the activation energy can be obtained by the Arrhenius plot. The energy barrier for the hydrogen-atom transition from the surface to the subsurface states and that for the bulk diffusion for jumping lattice interstitial sites are different.[34,36] Here, we investigate the reaction kinetics by measuring the frequency change to hydrogen with various concentrations at different temperatures. The results are shown in Fig. S2. Figure 5 shows the relationship between the hydrogen-gas concentration and the frequency slope at different temperatures from which we extracted the temperature dependence of k_a. The reaction constant k_a is described by the Arrhenius law,[51] $k_a = A_0 \exp(-E/k_B T)$, with E being the activation energy, k_B the Boltzmann constant, and A_0 the pre-exponential factor. As shown in the inset of Fig. 5, the Arrhenius plot yields the activation energy of 0.372 ± 0.003 eV, which is significantly larger than that for bulk diffusion (0.226 eV[52] and 0.23 eV[38]). However, our value is close to the activation energy for transition from surface to subsurface states (0.40 eV[36] and 0.43 eV[53]), indicating that the migration from the surface to the subsurface is the rate-limiting process during hydrogen absorption in our sensor system.

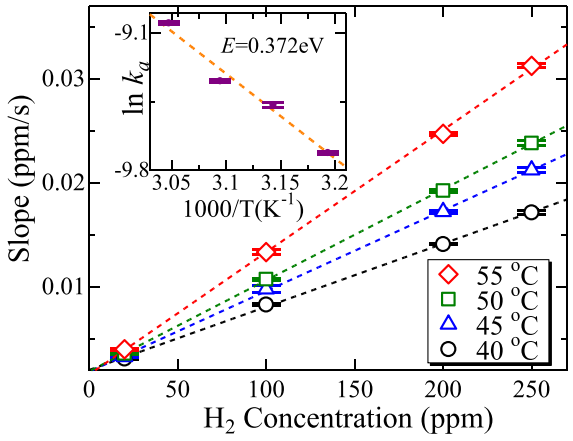

FIG. 5. Temperature dependence of the sensitivity of the 64.5 MHz resonator with various hydrogen-gas concentrations. The inset shows the Arrhenius plot, yielding the activation energy. The error bars indicate the standard deviation of three repeated experiments.

In summary, we proposed a highly sensitive hydrogen detection method using a wireless-electrodeless quartz-crystal resonator. A palladium film was deposited on a single side of the resonator as the sensing material. We observed the resonance-frequency decrease in the resonator and found that it arises from the geometry change induced by the palladium-film expansion. This sensing system achieved a lower detection limit of 1 ppm. We confirmed the nearly linear relationship between the frequency change and the resonator curvature by the FEM simulation. We then determined the activation energy of 0.372 eV for the hydrogen adsorption reaction into palladium, which is close to the activation energy for the surface-to-subsurface transition of the hydrogen atom. Our method thus demonstrates not only an important hydrogen-sensor application but also a basic study on interaction between hydrogen and palladium.

See the supplementary material for the comparison of frequency changes of the resonators with palladium films on one side and on both sides (Fig. S1), temperature dependence of the frequency response (Fig. S2), and details for the FEM simulation.

This research was supported by the Development of Advanced Measurement and Analysis Systems from the Japan Science and Technology Agency (Project No. JPMJSN16B5).

REFERENCES

[1]G. Korotcenkov, S. D. Han, and J. R. Stetter, Chem. Rev. **109**, 1402 (2009).
[2]T. Hübert, L. Boon-Brett, G. Black, and U. Banach, Sens. Actuators, B **157**, 329 (2011).
[3]C. S. Chang, M. Kotylev, and E. Ivanov, Appl. Phys. Lett. **102**, 142405 (2013).
[4]S. Öztürk and N. Kilinc, J. Alloys Compd. **674**, 179 (2016).
[5]T. Chen, Q. Wang, R. Chen, B. Zhang, K. P. Chen, M. Maklad, and P. R. Swinehart, Appl. Phys. Lett. **100**, 191105 (2012).
[6]G. B. Pour, L. F. Aval, and P. Esmaili, Sens. Rev. **39**, 622 (2019).
[7]G. B. Pour, L. F. Aval, M. N. Sarvi, S. F. Aval, and H. N. Fard, J. Mater. Sci.: Mater. Electron. **30**, 8145 (2019).
[8]F. D. Manchester, A. San-Martin, and J. M. Pitre, J. Phase Equilib. **15**, 62 (1994).
[9]R. Gremaud, M. Slaman, H. Schreuders, B. Dam, and R. Griessen, Appl. Phys. Lett. **91**, 231916 (2007).
[10]O. Dankert and A. Pundt, Appl. Phys. Lett. **81**, 1618–1620 (2002).
[11]N. Nakamura, T. Ueno, and H. Ogi, Appl. Phys. Lett. **114**, 201901 (2019).
[12]F. Favier, E. C. Walter, M. P. Zach, T. Benter, and R. M. Penner, Science **293**, 2227 (2001).
[13]S. Okuyama, Y. Mitobe, K. Okuyama, and K. Matsushita, Jpn. J. Appl. Phys., Part 1 **39**, 3584 (2000).
[14]Z. Y. Hu, T. Thundat, and R. J. Warmack, J. Appl. Phys. **90**, 427 (2001).
[15]J. Henriksson, L. G. Villanueva, and J. Brugger, Nanoscale **4**, 5059 (2012).
[16]M. Fisser, R. A. Badcock, P. D. Teal, and A. Hunze, Sens. Actuators, B **259**, 10 (2018).
[17]M. Fisser, R. A. Badcock, P. D. Teal, and A. Hunze, J. Lightwave Technol. **36**, 2166 (2018).
[18]T. Xu, M. P. Zach, Z. L. Xiao, D. Rosenmann, U. Welp, W. K. Kwok, and G. W. Crabtree, Appl. Phys. Lett. **86**, 203104 (2005).
[19]P. Offermans, H. D. Tong, C. J. M. van Rijn, P. Merken, S. H. Brongersma, and M. Crego-Calama, Appl. Phys. Lett. **94**, 223110 (2009).
[20]H. Ogi, Proc. Jpn. Acad., Ser. B **89**, 401 (2013).
[21]H. Ogi, K. Motohisa, T. Matsumoto, K. Hatanaka, and M. Hirao, Anal. Chem. **78**, 6903–6909 (2006).
[22]V. Pini, J. Tamayo, E. G. Santos, D. Ramos, P. Kosaka, H. D. Tong, C. V. Rijn, and M. Calleja, ACS Nano **5**, 4269 (2011).
[23]R. B. Karabalin, L. G. Villanueva, M. H. Matheny, J. E. Sader, and M. L. Roukes, Phys. Rev. Lett. **108**, 236101 (2012).
[24]W. P. Jakubik, M. W. Urbanczyk, S. Kochowski, and J. Bodzenta, Sens. Actuators, B **82**, 265 (2002).
[25]K. Yamanaka, N. Nakaso, D. Sim, and T. Fukiura, Acoust. Sci. Technol. **30**, 2 (2009).
[26]T. Yanagisawa, T. Ohgi, S. Akao, N. Nakaso, Y. Tsukahara, Y. Ohara, T. Tsuji, and K. Yamanaka, Appl. Phys. Lett. **98**, 123508 (2011).
[27]C. Gabrielli, P. P. Grand, A. Lasia, and H. Perrot, Electrochim. Acta **47**, 2199 (2002).
[28]X. M. H. Huang, M. Manolidis, S. C. Jun, and J. Hone, Appl. Phys. Lett. **86**, 143104 (2005).
[29]A. Borgschulte, F. Pendolino, R. Gremaud, and A. Züttel, Appl. Phys. Lett. **94**, 111907 (2009).
[30]H. Ogi, H. Nagai, Y. Fukunishi, M. Hirao, and M. Nishiyama, Anal. Chem. **81**, 8068 (2009).
[31]H. Ogi, M. Fujii, N. Nakamura, T. Shagawa, and M. Hirao, Appl. Phys. Lett. **90**, 191906 (2007).
[32]G. Sauerbrey, Z. Phys. **155**, 206 (1959).
[33]K. Ienaga, H. Takata, Y. Onishi, Y. Inagaki, H. Tsujii, T. Kimura, and T. Kawae, Appl. Phys. Lett. **106**, 021605 (2015).
[34]T. L. Ward and T. Dao, J. Membr. Sci. **153**, 211 (1999).
[35]J. E. Lennard-Jones, Trans. Faraday Soc. **28**, 333 (1932).
[36]P. Ferrin, S. Kandoi, A. U. Nilekara, and M. Mavrikakis, Surf. Sci. **606**, 679 (2012).
[37]R. J. Behm, V. Penka, M.-G. Cattania, K. Christmann, and G. Ertl, J. Chem. Phys. **78**, 7486 (1983).
[38]G. Alefeld and J. Volkl, *Hydrogen in Metals I* (Springer, Berlin, 1978), Chap. 12, pp. 321–326.
[39]A. Sieverts and W. Krumbhaar, Ber. Dtsch Chem. Ges. **43**, 893 (1910).
[40]R. C. Hughes and W. K. Schubert, J. Appl. Phys. **71**, 542 (1992).
[41]T. B. Flanagan, J. F. Lynch, J. D. Clewley, and B. Von Turkovich, J. Less-Common Met. **49**, 13 (1976).
[42]Y. Liu, X. Yu, R. Zhao, D. Shangguan, Z. Bo, and G. Liu, Biosens. Bioelectron. **19**, 9 (2003).
[43]H. Ogi, K. Motohisa, K. Hatanaka, T. Ohmori, M. Hirao, and M. Nishiyama, Biosens. Bioelectron. **22**, 3238 (2007).
[44]W. M. Mueller, J. P. Blackledge, and G. G. Libowitz, *Metal Hydrides* (Academic, New York, 1968), Chap. 12.
[45]L. B. Freund, J. A. Floro, and E. Chason, Appl. Phys. Lett. **74**, 1987 (1999).
[46]K. Yamanaka, S. Ishikawa, N. Nakaso, N. Takeda, D. Y. Sim, T. Mihara, A. Mizukami, I. Satoh, S. Akao, and Y. Tsukahara, IEEE Trans. Ultrason. Ferroelectr. Freq. Control **53**, 793 (2006).
[47]R. R. J. Maier, B. J. S. Jones, J. S. Barton, S. McCulloch, T. Allsop, J. D. C. Jones, and I. Bennion, J. Opt. A **9**, S45 (2007).
[48]B. Sharma and J. S. Kim, Int. J. Hydrogen Energy **42**, 25446 (2017).
[49]G. B. Pour and L. F. Aval, Results Phys. **7**, 1993 (2017).
[50]G. B. Pour and L. F. Aval, Nano **12**, 1750096 (2017).
[51]S. Arrhenius, *Über Die Dissociationswärme Und Den Einfluss Der Temperatur Auf Den Dissociationsgrad Der Elektrolyte* (Wilhelm Engelmann, Germany, 1889).
[52]Y. Fukai and H. Sugimoto, Adv. Phys. **34**, 263 (1985).
[53]R. Löber and D. Henning, Phys. Rev. B **55**, 4761 (1997).